Special Issue

Journal of Physical Organic Chemistry

Received: 14 November 2007, Revised: 12 August 2008, Accepted: 20 August 2008, Published online in Wiley InterScience: 26 September 2008

(www.interscience.wiley.com) DOI 10.1002/poc.1449

Structural and vibrational study of 2-(2′-furyl)-1*H*-imidazole

A. E. Ledesma[a], S. A. Brandán[a], J. Zinczuk[ba], O. E. Piro[ca], J. J. López González[d] and A. Ben Altabef[a]*,†

The 2-(2′-furyl)-1*H*-imidazole (1) has been prepared and characterized using infrared, Raman, and multidimensional nuclear magnetic resonance spectroscopies. Two conformations of this species obtained by rotation of 180°, approximately, around the C—C inter-ring bond are detected. Likewise, the crystal and molecular structure of 1 has been analyzed by X-ray diffraction methods and it evidenced that both conformations are present in the lattice with equal occupancy and linked in alternate way to the N—H---N bonded polymeric chains along the crystal [101] direction. Theoretical calculations have been carried out by employing the density functional theory (DFT)/B3LYP method, in order to optimize the geometry in gas phase of both conformers and to support the assignments of the vibrational bands of 1 to their normal modes. For a complete assignment of the compound, DFT calculations were combined with Pulay's SQMFF methodology in order to fit the theoretical frequency values to the experimental one. The nuclear magnetic resonance spectrum observed for 1 is successfully compared with the calculated chemicals shifts at B3LYP/6-311++G level of theory for the two conformers. Furthermore, natural bond orbital (NBO) analysis and topological (AIM) calculations for an oligomer, containing three alternated units of the N—H---N bonded chain found in the crystal, reveals the characteristics of the hydrogen bonds present in the polymeric structure. Copyright © 2008 John Wiley & Sons, Ltd.**

Supporting information may be found in the online version of this article.

Keywords: 2-(2′-furyl)-1*H*-imidazole; synthesis; crystal and molecular structure; vibrational spectra

INTRODUCTION

The aromatic heterocyclic compounds are of a great chemical interest because they are present in the skeleton of bio- and macromolecules. Thus, they have been widely studied in chemistry from different points of view. These molecules currently present complex spectra due to large size. The computational quantum chemistry has been extensively used as a tool to analyze, elucidate their molecular structures, and to carry out the assignment of the vibrational spectra.

The furylimidazoles compounds can be found as structural units of numerous types of drugs and polymers and for this they are of a great importance in biochemistry and pharmacology.[1–3] Recently, a chromophore that contains the furan and imidazole rings in its structure, isolated from the bovine serum albumin, was used as an adduct for the reaction of amino groups of proteins with glucose to form stable Amadori products without the aid of enzymes.[4] Moreover, (2-furyl) imidazoles have been used to study tautomeric preferences in histamines with great biological activity.[5] They are also important constituents in the synthesis reactions in organic chemistry.[6–9]

There are few data in the literature about molecular properties of furylimidazoles. Recently, Vázquez *et al.*[10] have reported the theoretical molecular structure of the isomeric series (2-furyl)-imidazoles using *ab initio* HF and MP2 calculations. So far, no data are available on the vibrational spectra of these compounds in the literature.

In the present work, we report the use of X-ray diffraction to determine the crystal structure of the 2 (2′-furyl)-1*H*-imidazole molecule (**1**). Moreover, theoretical density functional theory (DFT), natural bond orbital (NBO),[11–13] and topological (AIM)[14,15] calculations were performed to analyze the energies

* *Correspondence to: A. B. Altabef, Instituto de Química-Física, Facultad de Bioquímica, Química y Farmacia, Universidad Nacional de Tucumán, San Lorenzo 456, T4000CAN, S. M. de Tucumán, R. Argentina.*
E-mail: altabef@fbqf.unt.edu.ar

a *A. E. Ledesma, S. A. Brandán, A. B. Altabef*
Instituto de Química-Física, Facultad de Bioquímica, Química y Farmacia, Universidad Nacional de Tucumán, San Lorenzo 456, T4000CAN, S. M. de Tucumán, R. Argentina

b *J. Zinczuk*
Instituto de Química Orgánica de Síntesis (CONICET-UNR), Facultad de Ciencias Bioquímicas y Farmacéuticas, Suipacha 531, 2000 Rosario, Santa Fé, R. Argentina

c *O. E. Piro*
Departamento de Física, Facultad de Ciencias Exactas, Universidad Nacional de La Plata, Instituto IFLP (CONICET), C. C. 67, 1900 La Plata, R. Argentina

d *J. J. López González*
Departamento de Química Física y Analítica, Facultad de Ciencias Experimentales, Universidad de Jaén, 23071, Campus Las Lagunillas s/n, Jaén, España

† *Member of the Carrera del Investigador Científico, CONICET (R. Argentina).*

and the geometric parameters of its two conformers in the gas phase as well as the magnitude of the intramolecular interactions. Furthermore, the possible charge-transfer and the intermolecular bond path in a part of the polymeric chain in solid state formed by three alternated units of such conformers were analyzed. We have obtained crystals of this compound by improving the procedure proposed by Stoyanov *et al.*[16] In addition, the multidimensional NMR spectrum observed for **1** is successfully compared with the calculated chemical shift at B3LYP/6-311++G** level of theory for the two conformers.

IR and Raman spectra data and DFT/B3LYP/6-311++G** calculations for the two conformers of **1**, combined with Pulay's SQMFF methodology[17], have been used to carry out a complete and reliable vibrational analysis of the 2 (2′-furyl)-1*H*-imidazole. In order to investigate the stability of the most stable conformer, additional calculations of the electrostatic potential (ESP)[18,19] derived from atomic charges were performed for both conformers.

EXPERIMENTAL METHODS

The synthesis of **1** from 2-(2′-furyl)-4,5-1*H*-dihydroimidazole (J. Zinczuk, S. A. Brandán, O. Piro, A. E. Ledesma, J. J. López González, A. Ben Altabef, submitted). was reported by Stoyanov.[16] In the present work, a mixture of 2-(2′-furyl)-4,5-1*H*-dihydroimidazole (1.5 g, 11 mmol) and Pd/C 5% (400 mg) in dodecane (30 ml) was boiled, stirring for 3 h at 210 °C. The mixture was cooled, diluted with twice its volume of chloroform, and the catalyst filtered off. The solvent was removed under reduced pressure to give 1.050 g of a light brown solid residue and product mixtures were purified, using a silica 230–400 mesh, in a column chromatography of 3 cm diameter and 12 cm high. A mixture of hexane and ethyl acetate (1:1) and triethylamine (1%) was used as a mobile phase. Finally, the solid was crystallized in cool ethanol. Yield: 468 mg, 32%; m.p.: 168–169 °C. Literature[16]: 169.5–170 °C.

The solid state structure was solved by X-ray diffraction methods. The data were collected on an Enraf-Nonius CAD4 diffractometer with EXPRESS[20] and reduced with XCAD4.[21] The structure was solved by direct methods with a SHELXS[22] program and its non-H atom refined by full-matrix least-squares with SHELXL.[23] The hydrogen atoms were located in a difference Fourier map and isotropically refined at their found positions. The molecular plots of the compound (Figs. 1 and 2) were drawn with ORTEP.[24]

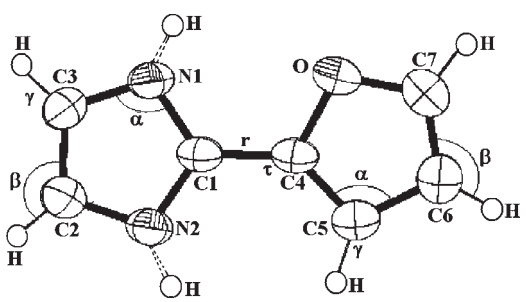

Figure 1. Molecular diagram of 2-(2′-furyl)-1*H*-imidazole showing the labeling of the non-H atoms and their ellipsoidal displacements at a 50% probability level. The N—H bonds are represented by dashed lines because both conformers are present in the crystalline structure

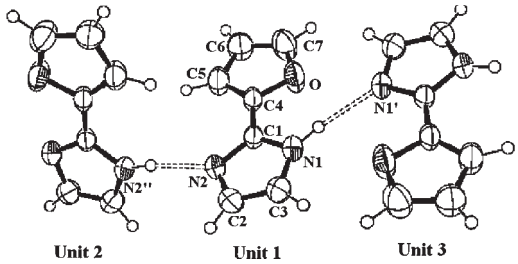

Figure 2. View of a N—H---N bonded polymer chain in solid 2-(2′-furyl)-1*H*-imidazole. The central monomer is related with the right and left side monomers through a crystallographic inversion center and a two fold axis rotation, respectively. The H-bonding is indicated by dashed lines

The infrared spectrum of the solid substance in KBr pellets, from 4000 to 200 cm^{-1} was recorded on a FTIR Bruker Vector 22 spectrophotometer, equipped with a Global source and DGTS detector with a resolution of 1 cm^{-1} and 200 scans. The Raman spectrum was recorded with a Bruker RF100/S spectrometer equipped with a Nd:YAG laser source (excitation line of 1064 nm, 800 mW of laser power) and a Ge detector at liquid nitrogen temperature. This last spectrum was recorded, likewise, with a resolution of 1 cm^{-1} and 200 scans. Nuclear magnetic resonance spectra were recorded for diluted solutions in DMSD-d_6 using a Bruker 400 FT spectrometer at 400 MHz. All spectra were measured at 300 K.

COMPUTATIONAL DETAILS

The potential energy curve associated with the rotation around the O—C4—C1—N1 dihedral angle (Fig. 1) for the molecule has been studied using the DFT method with the hybrid correlation functional B3LYP[25,26] with 6-31G* basis set, presenting in both cases two stable structures of C_S (planar) and C_1 (quasi planar) symmetries (Fig. 3). The optimized geometries for the two conformations of **1** in the curve of potential energy were obtained using the B3LYP method and the 6-31G*, 6-31G**, 6-311G*, and 6-311G** basis sets. NBO electron calculations for the two conformations of **1** were performed at the B3LYP/6-311++G** level using the NBO 3.1 program.[27] Atomic partial charges were calculated for both conformers from the ESP according to the Merz–Singh–Kollman Scheme [28] at the same level theory. All calculations were performed using the GAUSSIAN 03 program.[29] The use of molecular surfaces based on molecular electron density such as the molecular ESP[30,31] has a long tradition in the qualitative interpretation of the chemical reactivity and is very useful to elucidate molecular interactions.[19]

The force field in Cartesian coordinates calculated at B3LYP/6-311++G** level for the two stable conformations of **1** were useful to get their corresponding harmonic vibrational frequencies. The resulting force fields were transformed to 'natural' internal coordinates with the MOLVIB program.[32,33] The valence simple internal coordinates used for defining the above cited natural coordinates are shown in Fig. 1. The natural coordinates are shown in Table S1 (Supplementary Material) which were defined as proposed by Pulay *et al.*[17] with the labeling of the atoms corresponding to Fig. 1. Following the SQMFF procedure[34–37], the harmonic force field for two conformers of this compound evaluated at B3LYP/6-311++G** level were scaled

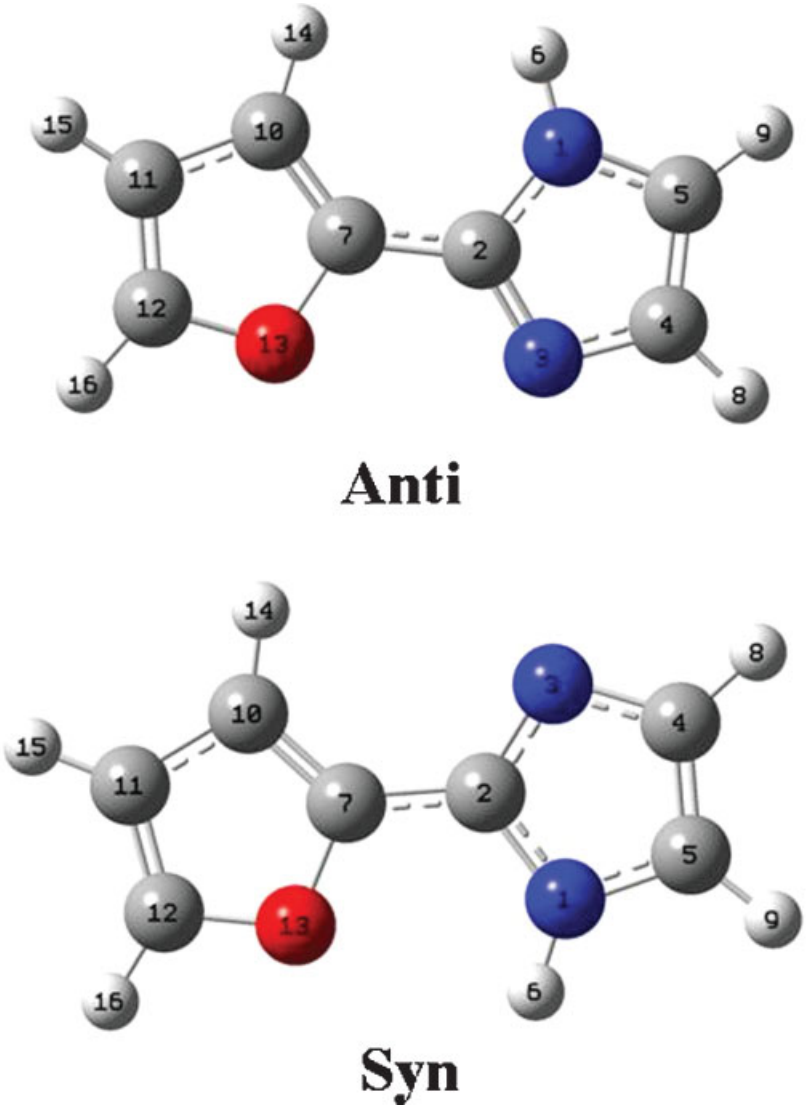

Figure 3. Theoretical structures and atoms numbering for anti (C_1) and syn (C_S) conformers of 2-(2′-furyl)-1*H*-imidazole.

transferring the recommended scaled factors of Rauhut and Pulay.[35,36] In order to get a better visualization of the nature of the different molecular vibrations of both conformers of **1**, the Gauss View program for molecular graphical representations was used.[38]

The calculated chemical shifts of the ^{1}H NMR and ^{13}C NMR for two conformers were obtained by GIAO method[39] using the B3LYP/6-311++G** level of theory, as it is routinely used for NMR chemical shift calculations on fairly large molecules.[40,41] The calculations have been performed using the geometries optimized for this level of theory and using TMS as reference.

The trimer species, with three units of both conformers linked alternately as shown in Fig. 2, was optimized at B3LYP/6-311++G** calculation and then, at this same level of theory, a NBO analysis was carried out. Moreover, for this species, the bond critical points (BCP) were topologically analyzed at B3LYP/6-311++G** level using the AIM 2000 program.[14,15] The total energy for trimer species using 6-311++G** basis set was corrected for basis set superposition error (BSSE) by the standard Boys–Bernardi counterpoise method.[42]

RESULT AND DISCUSSION

Structural analysis

Crystal and molecular structure

A summary of crystal data and refinement results for **1** are shown in Table 1. A molecular diagram of **1** is shown in Fig. 1. As expected, the molecule is planar (RMSD root mean square deviation of atoms from the least-squares plane equal to 0.053 Å). The comparison of the experimental geometrical parameters determined by X-ray diffraction in this work for **1** and reported from X-ray diffraction, too, for both imidazole and furan molecules[43,44] can be observed in Table 2. The formally double C(4)—C(5) and C(6)—C(7) bonds in the furyl group present lengths of 1.343(3) and 1.319(4) Å, being shorter than those of the formally single C(5)—C(6) bond [1.413(3) Å]. The experimental values of **1** are slightly different from those reported by others authors for both rings. It is important to observe that in **1** the lengths of the C—C and C═C bonds compared with the furan

Table 1. Crystal data and structure refinement results for 2-(2′-furyl)-1*H*-imidazole

Empirical formula	$C_7H_6N_2O$
Formula weight	134.14
Temperature	296 (2) K
Wavelength	1.54184 Å
Crystal system, space group	Monoclinic, C2/c (# 15)
Unit cell dimensions	$a = 20.259$ (2) Å
	$b = 5.793$ (1) Å
	$c = 12.006$ (2) Å
	$\beta = 112.54$ (1)°
Volume	1301.4 (3) Å^3
Z, calculated density	8, 1.369 Mg/m^3
Crystal size	$0.22 \times 0.20 \times 0.20$ mm^3
(range for data collection	4.73–67.92°
Reflections collected/unique	1453/1146 [R(int) = 0.0434]
Observed reflections [$I > 2\sigma(I)$]	1002
Final *R* indices[a] [$I > 2\sigma(I)$]	$R_1 = 0.0525$, $wR_2 = 0.1476$
R indices (all data)	$R_1 = 0.0581$, $wR_2 = 0.1557$
Largest peak and hole	0.250 and −0.242 e.A^{-3}

[a] *R* indices defined as $R_1 = \Sigma||F_o| - |F_c||/\Sigma|F_o|$ and $wR_2 = [\Sigma w(|F_o|^2 - |F_c|^2)^2/\Sigma w(|F_o|^2)^2]^{1/2}$.

Table 2. Experimental geometrical parameters (bond distances in Å and bond angles in degrees) for the 2-(2′-furyl)-1*H*-imidazole*, imidazole, and furan molecules

Parameter[a]	Furan[b]	Imidazole[c]	This work*
	Bond lengths (Å)		
O—C(7)	1.368(6)	—	1.363 (3)
O—C(4)	1.368(6)	—	1.361 (2)
C(4)—C(5)	1.322(6)	—	1.343 (3)
C(5)—C(6)	1.428(3)	—	1.413 (3)
C(6)—C(7)	1.322(6)	—	1.319 (4)
N(1)—C(1)	—	1.313 (30)	1.342 (3)
N(1)—C(3)	—	1.382 (30)	1.374 (3)
N(2)—C(1)	—	1.364 (30)	1.339 (2)
N(2)—C(2)	—	1.377 (30)	1.369 (3)
C(2)—C(3)	—	1.364 (30)	1.345 (3)
	Bond angles (°)		
C(7)—O—C(4)	106.17 (60)	—	106.6 (2)
C(5)—C(4)—O	110.14 (40)	—	109.2 (2)
C(4)—C(5)—C(6)	106.76 (24)	—	107.1 (2)
C(7)—C(6)—C(5)	106.76 (24)	—	106.6 (2)
C(6)—C(7)—O	110.14 (40)	—	110.6 (2)
C(1)—N(1)—C(3)	—	104.93	105.6 (2)
C(1)—N(2)—C(2)	—	106.90	105.7 (2)
N(1)—C(1)—N(2)	—	111.99	111.6 (2)
N(2)—C(2)—C(3)		105.48	108.7 (2)
N(1)—C(3)—C(2)		110.69	108.4 (2)

[a] The labeling of the atoms is the corresponding to Fig. 1.
[b] Reference [44].
[c] Reference [43].

molecule are between 0.003 and 0.021 Å, while the C—O distance practically is not altered by the imidazolic part. On the other hand, the lengths C—N and C=C of the imidazolic part in **1** cannot be compared with the corresponding lengths of imidazole molecule due to the fact that experimental lengths in this compound are an average of the two conformations.

All but the nitrogen H-atoms fulfill the requirements of the symmetric center for the C2/c space group. Both conformers are present in the lattice with equal occupancy and alternated arrangement in the N—H---N bonded polymeric chains along the crystal [101] direction. Only three units of the polymeric structure are shown in Fig. 2. A given monomer (unit 1) on a chain is on one side H-bonded to an inversion related molecule (unit 3) [d(N1H---N1′) = 2.049 Å, <(N1—H---N1′) = 164.9°] and on the other side (unit 2) to a twofold rotation related one [d(N2″H---N2) = 1.972 Å, <(N2″—H---N2) = 164.7°]. These results are closer to the obtained values for related molecules.[45–47] This arrangement implies a slight crystal symmetry breaking by the nitrogen H-atoms of both inversion centers and the twofold rotation axes of the C2/c group. Crystallographic data for the structure were deposited into the Cambridge Crystallographic Data Center as supplementary publication number CCDC 665861.

Geometry optimization

The calculated potential energy curve using the DFT/B3LYP/6-31G* method as mentioned in step 3 was performed. Two different stable conformations were obtained according to syn and anti position of oxygen atom with respect to the N—H bond, named syn (C_S) and anti (C_1) conformers, respectively. The labeling of the atoms for both conformers is showed in Fig. 3. The energy differences among them at this calculation level (3.85 kcal/mol) are lightly next to those reported for these compounds with the MP2 method (3.38 kcal/mol) by Vázquez *et al.*[10] The energy barrier is higher in *ca.* 2.0 kcal/mol for DFT/B3LYP compared to the MP2 method. These values are closer to the typical sp^3 carbon atoms bonds (3.2 kcal mol^{-1}) than to the value for such a bond in typical conjugated system (7 kcal mol^{-1}).[48] A similar result has been obtained for the styrene molecule by Granadino-Roldán *et al.*[49] The total and relative energies of the two stable conformations of **1** for different basis sets are presented in Table S2. In all cases, the calculations predict that the energy of the syn conformer is lower than the one corresponding to anti conformer in the approximation of the isolated molecule in gas phase while the X-ray analysis indicate that both conformations are present with equal population in the solid phase.

The calculated parameters for both conformers with the B3LYP levels of theory at different basis sets and the corresponding standard deviations expressed as the RMSD are listed in Table S3. In general, for the two optimized conformations, the results with the different theoretical calculation employed are in reasonable agreement among them and also with those values obtained from the X-ray data. The standard deviation for the geometrical parameters for all the calculation levels used are practically independent of the basis set employed. The calculations predict values for the O13—C7—C2—N1 and C10—C7—C2—N3 dihedral angles of 179.7° in the anti conformer while the values

for the C10—C7—C2—N1 and O13—C7—C2—N3 dihedral angles are 0.3°. In the syn conformer the two rings are coplanar with dihedral angles of 180°.The stability of the syn conformer in relation to the anti conformer was investigated using the ESP maps [18,19] because these surfaces are important for describing overall molecular charge distributions as well as anticipating sites of electrophilic addition.[19] The molecular ESP values for two conformers using 6-31G* and 6-311++G** basis sets are given in Table S4 while Fig. 4 shows the ESP maps for anti and syn conformers. The red color represents negatively charged areas of the surface (i.e., those areas where accepting an electrophile is most favorable). The atomic charges derived from the ESPs (MK) and natural atomic charges were also analyzed and the corresponding values are given in Table S5. Note that both charges are very similar, except the MK charges for both conformers using 6-311++G** basis set. The important factor responsible for the lesser stability of the anti conformer is the electrostatic repulsion between the two lone pairs on N3 and O13. Hence, a strong red color on both atoms is observed in the corresponding Fig. 4. On the other hand, in the syn conformer the two eclipsed C10–H14 and N1–H6 bonds are absent and only a red color on the N3 atom of the imidazoline ring is observed. Moreover, the electrostatic repulsion between N3 and O13 is replaced by a decreased repulsion between N1 and O13 (the N1–O13 distance in this conformer is shorter than in C1 (N1–O13 2.79–2.8 Å) and by a possible stabilizing electrostatic interaction between O13 and H6 (distance O13–H6 2.5 Å). For the anti conformer the dipolar moment value is 4.08 D, while in the syn conformer the dipolar moment is 2.91 D (Figure S1 of the Supporting Material). The elevated value of the dipolar moment for the anti conformer could explain its experimental stability, as observed by Sambrano *et al.*[50] for the M4 tautomer of 5-methylcytosine and by Brandán *et al.*[51] for the imino-hidroxy tautomer of 1,5-dimethylcytosine.

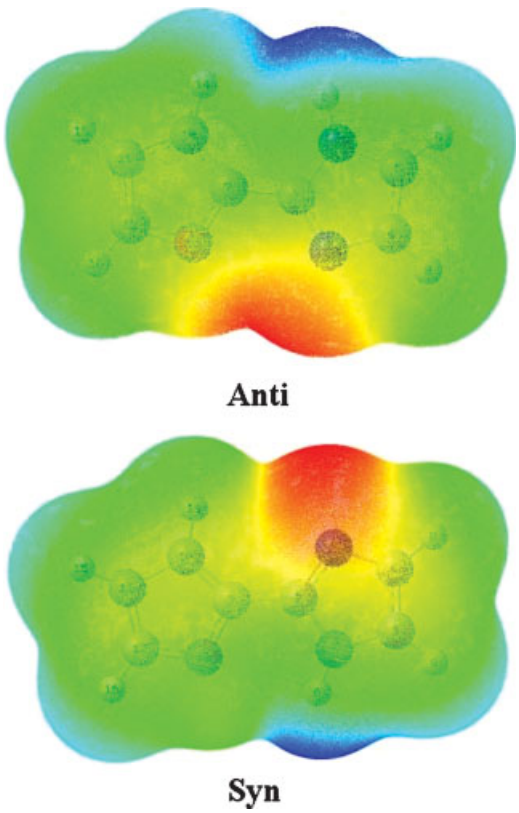

Figure 4. Calculated electrostatic potential surfaces on the molecular surfaces of anti and syn conformers of 2-(2′-furyl)-1*H*-imidazole. Color ranges, in a.u.: from red −0.09 to blue +0.09. B3LYP functional and 6-31G* basis set. Isodensity value of 0.005.

NBO analysis

The stability of the conformers of **1** was also investigated by NBO calculations[11–13,25]. The energies and occupancies of bond orbital and the lone pairs of oxygen and nitrogen atoms for the two conformers are presented in Table S6. The second order perturbation energies $E^{(2)}$ (donor → acceptor) that involve the most important delocalization are given in Table 3. After a careful analysis of the results, we found that the contribution of the $\Delta E^{(2)}_{\sigma-\sigma*}$ and $\Delta E^{(2)}_{\pi-\pi*}$ are higher for anti conformer than syn conformer. The stabilizations energies for the LP(1)N1 → π*C2—N3 and LP(1)N1 → π*C4—C5 charge-transfers are greater for syn conformer than anti conformer while a contrary effect for the stabilization energies of lone pairs of the O atom for syn conformer is observed (Table 3). The energies for the charge-transfer from the lone pair of the O atom are smaller than the corresponding ones to the N atom, in agreement with the larger electronegativity of the O atom, as was observed by Alabugin *et al.*[52] for six-member saturated heterocycles and cyclohexane.

For the trimer species, the energies and occupancies of the NBO orbitals and two contributions (LP(1)N(2) → σ^* N(2″)—H and

Table 3. Stabilization energies ($E^{(2)}$) associated with main delocalizations of 2-(2′-furyl)-1*H*-imidazole

	$E^{(2)}$ (kcal/mol)	
(Donor → acceptor)	Anti	Syn
σC2—C7 → σ*N1—C2	0.70	1.04
σC2—C7 → σ*C2═N3	3.05	2.69
σC2—C7 → σ*C7═C10	4.92	3.99
σC7═C10 → σ*C2—C7	5.23	4.65
σC7—O13 → σ*C7═C10	1.12	0.83
πC2═N3 → π*C7═C10	11.91	10.69
πC4═C5 → π*C2═N3	13.73	13.42
πC7═C10 → π*C11═C12	16.15	16.91
π*C2═N3 → π*C4═C5 (#)	—	167.61
π*C2═N3→π*C7═C10 (#)	—	191.78
LP(1)N1 → π*C2═N3	46.50	48.55
LP(1)N1 → π*C4═C5	30.80	31.11
LP(1)O13 → σ*C2—C7	0.99	0.78
LP(1)O13 → σ*C11═C12	3.05	2.81
LP(2)O13 → π*C7═C10	28.91	26.17
LP(2)O13 → π*C11═C12	27.61	25.64

(#), the elevated values of $E^{(2)}$ in the syn conformer not explain the higher stability of syn conformer because the occupancies are the same in both conformers (see Table S6).

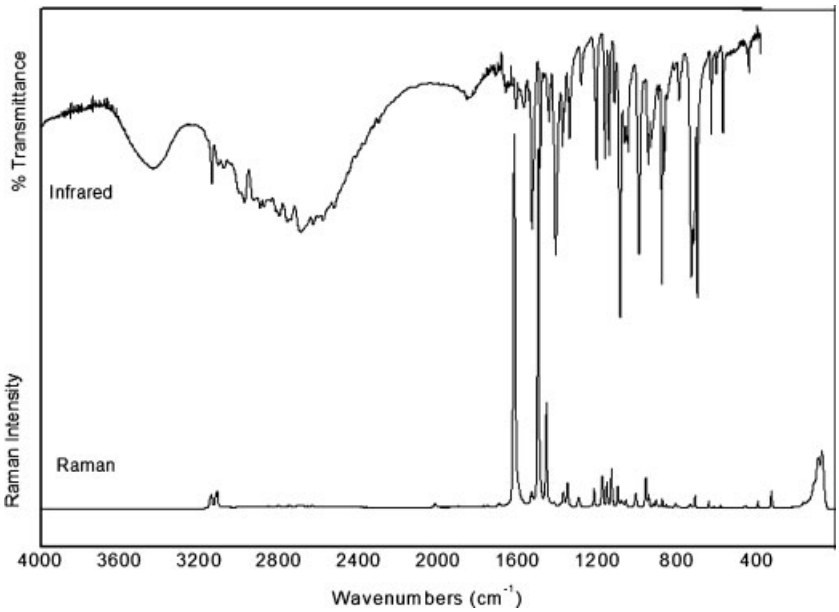

Figure 5. Infrared (upper) and Raman spectra (bottom) of the solid substance

LP(1)N(1′) → σ^* N(1)—H) to the delocalization energy (Fig. 2) are shown in Table S7. The NBO analysis predicts different charges for each monomer unit in the H-bonded trimer. Unit 3 presents a slightly positive charge (0.04315 a.u.); unit 2 presents a negative charge (−0.04435 a.u.) while unit 1 presents a practically null charge (0.00122 a.u.). For those first contributions, the N2 atom of unit 1 is an electron charge donor and the H atom bonded to N2″ of unit 2 is an acceptor while for the second contribution, the H atom bonded to N1 of unit 1 is an acceptor and the N1′ atom of unit 3 is an electron charge donor. The occupancies of the σ^*N—H antibonding orbital in the trimer are higher than in the monomers (Table S7) and their corresponding energy shows the same tendency.

Topological analysis for the H-bonded trimer species

The existence of bond paths between three alternated monomer units in **1** was examined employing the AIM program. We focused our attention on the H-bonded trimer as shown in Fig. 2, optimizing its geometry at B3LYP/6-311++G** level. In Table S8, the main topological properties obtained by the AIM program for two critical points N2(1)---H—N2″(2) and N1′(3)---H—N1(1) are shown. The experimental N—H---N bond lengths in the solid have been also included in the same Table and are compared with the corresponding calculated bond lengths. Both distances predicted by calculations are similar between them, but smaller than the obtained values from the X-ray data (1.972 Å for N2(1)---H—N2″(2) bond length and 2.049 Å for N1′(3)---H—N1(1) bond length). Also, the calculated electron density values for each critical point are 0.0326 and 0.0307 a.u., respectively. Moreover, the above mentioned charge-transfers for the 2-(2′-furyl)-1*H*-imidazole could contribute to the electron properties in conjugated rings, as in the furan molecule reported by Montejo *et al.*[53] These results are in excellent agreement with the NBO properties analyzed in the previous section.

Vibrational analysis

The experimental structural analysis show that the anti and syn conformers appear with the same population in the solid phase of **1**. Thus, the bands associated to the different normal modes of both monomers should be observed in the vibrational spectra of the solid. For a complete assignment of the experimental bands of 2-(2′-furyl)-1*H*-imidazole, the theoretical calculations for each conformer at the B3LYP/6-311++G** level combined with Pulay's SQMFF methodology[34–36] and a comparison with related molecules[54–57] were considered. Both conformers have 42 normal modes of vibration active both in infrared and Raman spectra. For the anti conformer those modes are arranged by symmetry species: 29 A′ + 13 A″ while for the syn conformer all modes have A symmetry. The recorded infrared and Raman spectra in solid phase for **1** are shown in Fig. 5. The average IR spectrum of the two monomers was simulated (Fig. 6) by summing the population-weight of both conformers calculated by using B3LYP/6-311++G** frequencies and intensities in a similar form to the one employed by Tuttolomondo *et al.*[58] for $CH_3SO_2OCH_2CH_3$. This calculated spectrum reproduces the experimental spectrum reasonably well, and for the agreement between the observed IR spectrum and the calculated one taking into account the conformational population, thus let us concludes that both conformers are present in the solid phase. The assignments of the vibrational normal modes for the two conformers are shown in Table 4.

In general, all modes are strongly mixed among them. We discuss below the assignment of the bands for both conformers of the compound in two spectral regions.

Assignment of the bands

Region 4000–1000 cm^{-1}. The broad band observed in the infrared spectra at 3440 cm^{-1} can be assigned to the N—H stretching vibration. The form of this band shows the probability

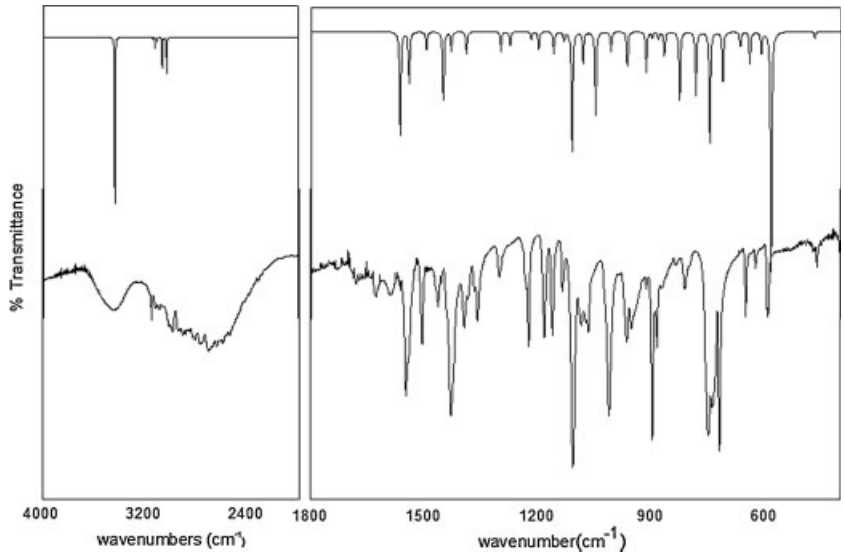

Figure 6. Comparison between the refined average calculated (upper) and experimental infrared spectra (bottom) of 2-(2′-furyl)-1*H*-imidazole. The calculated spectrum was obtained from B3LYP/6-311++G** using average frequencies and intensities for both conformers

of the H bonding, as observed in the X-ray data. The group of bands in the 3150–3000 cm^{-1} region in the infrared and Raman spectra of the solid substance can be assigned to C—H stretching modes. The bands at 3149, 3118, 3109, 3088, and 3011 cm^{-1} are associated to them. These bands appear shifted at lower frequencies in relation to the furan and imidazole molecules. The numerous bands between 3000 and 2200 cm^{-1} can be attributed to O---H hydrogen bonding formed by spatial arrangement of the molecules in the polymeric chains along the lattice crystal as shown in the molecular packing of the Figure S2.

The bands at 1625 and 1504 cm^{-1} were mainly assigned to C═C stretchings of the furanic part associated to both conformers. The corresponding C═C stretchings of the imidazolic part are assigned to the bands at 1547/1538 cm^{-1} associated with syn and anti conformers, respectively.

In agreement with the calculation, the bands at 1462/1453 cm^{-1} in the infrared spectrum of solid phase were assigned to N═C stretching modes for anti and syn conformers, respectively.

The three C—N stretchings are assigned to the pairs of bands at 1428/1393, 1365/1358, and 1159/1133 cm^{-1} as can be seen in Table 4. The band at 1380 cm^{-1} in the IR spectrum is mainly, for their P.E.D. contribution associated to C—C stretching mode for both conformers.

In 1300–1000 cm^{-1} region, the in plane deformation, βC—H and the C—O stretching modes are expected. The bands observed at 1300/1260; 1229/1222; 1106/1102; 1084; and 1010 cm^{-1} are associated to βC—H modes of both conformers while the bands at 1181 and 1075 cm^{-1} are related to C—O stretchings. The IR band at 1065 cm^{-1} is associated to in plane deformation, βN—H for two conformers as shown in Table 4.

Region below 1000 cm^{-1}. In this region, the imidazole and furan deformation rings are predicted for the calculation with higher P.E.D. contribution. Hence, the pairs of bands at 965/952 and 927/911 cm^{-1} are associated to the βR_1 (i) and βR_2 (i) modes of the imidazolic part for both conformers. The furan βR_1 (f) and βR_2 (f) deformation modes for two conformers are assigned to the bands at 897 and 894 cm^{-1}, respectively. One important observation is that the experimental frequencies difference between the two imidazole deformation ring modes for the compound is 41 cm^{-1}, in agreement to the reported value by King *et al.*[55] for the imidazole molecule (40 cm^{-1}).

The five IR bands between 883 and 719 cm^{-1} are easily assigned to the C—H out of plane deformation, γC—H, for the two conformers because are clearly predicted by the theoretical calculations, as shown in Table 4.

In accordance to the frequencies reported at 603 and 600 cm^{-1} by Klots *et al.*[56] for the two furan ring torsions, the bands at 665 and 650 cm^{-1} were assigned to torsion modes for both conformers. For the imidazole ring those modes were assigned to the pairs of bands at 624/622 and 593/591 cm^{-1}. Newly, the observed frequencies difference between the two imidazole torsion ring modes for the compound is 31 cm^{-1}, according to the reported value by King *et al.*[55] for the imidazole molecule (30 cm^{-1}).

The N—H out of plane deformation modes, γN—H, are predicted for two conformers at different frequencies, therefore, both modes are assigned to the bands at 524 and 470 cm^{-1} for syn and anti conformers, respectively.

The remaining inter-ring modes are observed at lower frequencies. The two expected inter-ring bending, βC—C of the two conformers were assigned indistinctly, to the IR band at 461 cm^{-1} and the Raman band at 153 cm^{-1}. The calculations predict the inter-ring C—C stretching mode for anti conformer at 388 cm^{-1} and for syn conformer at 392 cm^{-1}, for this reason the band observed at 402 cm^{-1} in the infrared spectrum is assigned to these modes.

Finally, the shoulder observed in the Raman spectrum at 119 cm^{-1} was assigned to the butterfly mode, defined by Fogarasi *et al.*[59] for the two rings systems. As the calculations

Table 4. Experimental[a] and calculated[b] (B3LYP/6-311++G** level) frequencies (cm^{-1}) of 2-(2′-furyl)-1*H*-imidazole

Mode	Symmetry		Infrared[a]	Raman[a]	SQM[b]	SQM[b]	Assignments[c]
	Anti	Syn	Solid	Solid	Anti	Syn	
1	A	A′	3440 br		3440	3440	ν(N2—H) (99)
2	A	A′	3149 w	3148 (4)	3147	3150	ν(C2—H2) (88), ν(C3—H3) (11)
3	A	A′	3118 vw	3126 (4)	3117	3118	ν(C3—H3) (88), ν(C2—H2) (11)
4	A	A′	3109 vw	3108 (5)	3114	3107	ν(C5—H5) (97)
5	A	A′	3088 vw	3086 (1)	3089	3066	ν(C7—H7) (86), ν(C6—H6) (11)
6	A	A′	3011 vw	3005 (1)	3011	3034	ν(C6—H6) (89), ν(C7—H7) (12)
7	A	A′	1625 w	1626 (100)	1619	1634	ν(C4═C5) (41), ν(C6═C7) (22)
8		A′	1547 vs			1538	ν(C6═C7) (50)
	A		1538 vs	1539 (4)	1538		ν(C3═C2) (26), ν(C6═C7) (19)
9	A	A′	1504 s	1505 (96)	1503	1501	ν(C6═C7)(29), ν(C1═N1)(14)
10	A		1462 m	1464 (29)	1460		ν(C1═N1) (22), ν(C4═C5) (16), β(C7—H7) (15)
		A′	1453 w	1454 (2)		1436	ν(C1═N1) (20), β(C6—H6)(11)
11	A		1428 vs	1428 (2)	1423		ν(C1—N2) (23), β(C6—H6)(19)
		A′	1393 m	—		1399	ν(C1—N2) (20), ν(O—C7) (11)
12	A	A′	1380 w	1380 (4)	1377	1375	ν(C5—C6) (20), β(C6—H6)(14)
13		A′	1365 w			1365	ν(C3—N1) (26), ν(C1═N1) (18), β(N2—H) (14)
	A		1358 m	1358(7)	1355		ν(C3—N1) (20), ν(C1═N1) (12)
14		A′	1300 m	1303 (3)		1277	β(C7—H7) (20), ν(C5—C6) (14)
	A		1260 sh	1226 (5)	1258		β(C7—H7) (31), β(C6—H6) (11)
15	A		1229 m		1227		β(C5—H5) (31), β(C7—H7) (12)
		A′	1222 s			1217	β(C5—H5) (27), ν(O—C4) (26)
16	A	A′	1181 s	1184 (8)	1177	1166	ν(O—C7) (22), β(C6—H6) (18)
17		A′	1159 s	1160 (7)		1161	ν(C2—N2) (29), β(C2—H2) (17), ν(C1—N2) (16)
	A		1133 m	1138 (10)	1148		ν(C2—N2) (43), β(C5—H5) (23)
18		A′	1106 vs	1106 (6)		1119	β(C2—H2) (17), β(C3—H3) (13)
	A		1102 s		1111		β(C2—H2) (23), β(C3—H3) (12)
19	A	A′	1084 w	1091 sh	1086	1081	β(C3—H3) (28), β(C2—H2) (12)
20	A	A′	1075 w	1065 (2)	1076	1069	ν(O—C4) (49), ν(C5—C6) (20)
21	A	A′	1065 w	1065 (2)	1052	1062	β(N2—H) (32), ν(C2—N2) (29)
22	A	A′	1010 vs	1015 (4)	1011	1004	β(C6—H6) (29), β(C2—H2) (27)
23	A		965 m	965 (8)	962		βR_1 (i) (44)
		A′	952 m	950 (4)		955	βR_1 (i) (53), β(C3—H3) (10)
24		A′	927 w			923	βR_2 (i) (51), βR_2 (f) (19)
	A		911 w	913 (3)	921		βR_2 (i) (47), βR_1 (i) (19)
25	A	A′	897 vs		896	894	βR_1 (f) (56), βR_2 (f) (36)

(continues)

Table 4. (Continued)

Mode	Symmetry		Infrared[a]	Raman[a]	SQM[b]	SQM[b]	Assignments[c]
	Anti	Syn	Solid	Solid	Anti	Syn	
26	A	A″		894 (2)	895	889	βR_2 (f) (62), βR_2 (i) (29)
27		A″	883 m	882 (2)		883	γ(C2—H2) (32), γ(C5—H5) (31)
	A		862 w	863 (1)	865		γ(C2—H2) (55), γ(C7—H7) (30), τR_1 (f) (15)
28	A			843 (1)	857		γ(C3—H3) (83), τR_1 (i) (10)
		A″	835 w			854	γ(C3—H3) (51), γ(C6—H6) (18)
29		A″	810 m	816 (1)		822	γ(C5—H5) (42), γ(C7—H7) (32)
	A		797 w		789		γ(C5—H5) (58), γ(C7—H7) (15)
30	A		748 vs	743 (1)	735		γ(C7—H7) (43), γ(C2—H2) (21), γ(C5—H5) (12)
		A″	733 s			733	γ(C7—H7) (57), Butt (11)
31	A	A″	719 vs	717 (3)	722	719	γ(C6—H6) (68), γ(C3—H3) (24)
32	A	A″	665 w		663	667	τR_1 (f) (42), τR_2 (f) (21), Butt (15)
33	A	A″	650 m	648 (2)	648	649	τR_2 (f) (37), Butt (26), τR_2 (i) (15)
34		A″	624 w	624 (1)		623	τR_1 (i) (42), τR_2 (f) (21)
	A		622 w		620		τR_1 (i) (35), τR_2 (f) (26)
35	A		593 w		595		τR_2 (i) (56), τR_2 (f) (26)
		A″	591 w	591 (1)		590	τR_2 (i) (46), τR_2 (f) (40)
36		A″	524 w			545	γ(N2—H) (40), τR_2 (i) (40)
	A		470 w		487		γ(N2—H) (71), τR_2 (i) (19)
37	A	A′	461 w	461 (1)	458	460	β(C1—C4) (35), β(C4—C1) (33)
38	A	A′	402 w	402 (2)	390	393	ν(C1—C4) (48), βR_2 (f) (12)
39	A	A″	333 w	334 (4)	313	314	γ(C4—C1) (48), τR_2 (i) (17), τR_2 (f) (14)
40	A	A′		153 sh	144	141	β(C4—C1) (50), β(C1—C4) (47)
41	A	A′		119 sh	119	119	Butt (64), γ(C4—C1) (33)
42	A	A′		81 (15)	20	70	τ(C4—C1) (61), γ(N2—H) (17)

Abbreviations: s, strong; m, medium; w, weak; v, very; sh, shoulder; br, broad.
[c] P.E.D. is given in parenthesis and contributions only $\geq$10% were considered.

Table 5. Scaling factors force fields of 2-(2′-furyl)-1*H*-imidazole

	Initial values[a]	Final values[b]	
Coordinates	Anti, syn	Anti	Syn
νN—H	0.887	0.887	0.887
νC—H	0.919	0.903	0.900
νC—C	0.923	0.973	0.960
νC═C	0.923	0.976	0.959
νC—N	0.923	0.963	0.961
νC═N	0.923	0.963	0.961
νC—O	0.923	0.973	0.960
βN—H	0.887	0.890	0.874
βC—H	0.951	0.951	0.951
βC—C	0.995	0.995	0.995
βR	0.995	0.985	0.984
τR	0.942	0.974	0.958
γC—H	0.975	0.975	0.978
γN—H	0.975	0.975	0.979
γC—C	0.942	0.942	0.942
Butt	0.942	0.995	0.995
τR	0.942	0.942	0.942

Abbreviations: ν, stretching; β, in the plane deformation, βR, ring deformation; γ, out of plane deformation; τR, ring torsion; Butt, butterfly

[a] References [35,36].

[b] This work.

Table 6. Scaled force constants of 2-(2′-furyl)-1*H*-imidazole

	2-(2′-Furyl)-1 *H*-Imidazole[a]			
Description	Anti	Syn	Furan[a]	Imidazole[a]
f (C—C)	5.57	5.44	5.56	—
f (C═C)	7.93	7.49	7.91	752
f (C—N)	5.89	6.47	—	6.29
f (C═N)	7.25	7.92	—	8.24
f (N—H)	6.55	6.55	—	6.84
f (C—H)	5.23	5.23	5.42	5.39
f (C—O)	6.38	6.36	5.66	—
βR	0.37	0.47	0.38	0.40
τR	0.66	0.68	0.60	0.70
f (βC—H)	0.49	0.48	0.45	0.46
f (βN—H)	0.55	0.47	—	0.44
f (γC—H)	0.36	0.37	0.36	0.36
f (γN—H)	0.13	0.19	—	0.17
f (τ Butt)	0.75	0.82	—	—
f (τw ring)	0.03	0.10	—	—

Units in mdyn $Å^{-1}$ for stretching and mdyn Å rad^{-2} for angle deformations.

[a] Calculated at DFT/B3LYP/6-311++G** level theory in this work.

predict, the band observed in the Raman spectrum at 81 cm^{-1} can be assigned to the inter-ring τC—C twisting mode.

The vibrational analysis shows that, in general, the observed frequencies for the compound are shifted toward lower frequencies than the corresponding reported for the furan and imidazole molecules. This fact can be related to the hyperconjugation effect, which is higher in this compound than the furan and imidazole molecules.

Force field

The scaling procedure was made following the method described in the computational details section. The RMSD obtained comparing the experimental and calculated frequencies from B3LYP/6-311++G** are 70.0 cm^{-1} for anti conformer and 69.7 cm^{-1} for the other conformer, which were decreased until 25.0 and 22.9 cm^{-1} respectively, when using the scale factors from References [35,36] and, finally until 12.3 and 9.1 cm^{-1}, respectively, when using the final scale factors from the refinement to the experimental data. The initial and final scale factors values are observed in Table 5. We can see that only a few modes have a participation of $\geq$50% of a single coordinate, whereas other modes represent very complex vibrations in which several coordinates are involved. The SQM force field was employed to calculate the internal force constants which are compared with the corresponding calculated values of the furan and imidazole compounds at B3LYP/6-311++G** level. The scaled force constants are given in Table 6. The comparison among them shows that in general the force constants of the 2-(2′-furyl)-1*H*-imidazole compound are in agreement with those calculated by us in this work for the furan and imidazole compounds. The observed differences could be attributed to the strong hyperconjugatives effects between the two rings.

NMR results

A comparison between the experimental and calculated chemical shifts for the C and H atoms are given in Tables S9 and S10, respectively. The comparison shows that the calculated ^{13}C chemical shifts from CSGT are in accordance with the experimental values, while the closest values were obtained with the GIAO method and the 6-311++G** basis set. Furthermore, the calculated shifts with all methods for the C(2), C(7), and C(1) atoms are higher than the experimental values. One important observation is that the results obtained from the conformational average have better agreement with data experimental, as expected, due to the presence of the two conformers in the solution. On the other hand, the calculated shifts with the two methods used for the H atom show significant differences with the experimental results. The addition of the polarization and diffuses functions at the basis set improves the results; however, the CSGT method predicts shifts fairly different than the GIAO method for this atom. This disparity would be attributed to the fact that the GIAO method uses basis functions which depend on the field while the CSGT method achieves gauge invariance by performing a continuous set of gauge transformations, for each point, obtaining an accurately description of the current density.[40,41]

CONCLUSIONS

We summarize here the main conclusions of the present work:

- We have determined the crystal and molecular structure of the substance by X-ray diffraction methods and characterized it by infrared and Raman spectroscopic techniques in the solid state and also by NMR in solution.
- DFT calculations suggest the existence of two molecular conformations syn (C_1) and anti (C_S), being the Cs conformation the most stable in gas phase, while in solid phase and solution the two conformations are in equal populations.
- Neither the calculated equilibrium energy nor the computed bond lengths and angles of the two conformers show significant variations with the different basis sets employed.
- The differences in the stability between both conformers were explained in terms of the partial charges of the atoms determined from the best fit of the ESP of each molecule.
- The present work reveals the existence of intermolecular contacts between adjacent molecules in the crystal, as observed by the X-ray diffraction results. Those intermolecular contacts have been interpreted by NBO and topological analysis calculations.
- The calculated harmonic vibrational frequencies for **1** are consistent with the observed solid state infrared and Raman spectra. The presence in the crystal of both conformers was detected in the IR spectrum and a complete assignment of the vibrational modes was accomplished.
- An SQM force field was obtained for syn and anti conformers of 2-(2′-furyl)-1*H*-imidazole after adjusting the theoretically obtained force constants to minimize the difference between observed and calculated frequencies.

Acknowledgements

S. A. Brandán thanks for the grant from Beca Banco Rio. The authors thank Prof. Tom Sundius for making available to us the MOLVIB Program. We also thank CONICET (Consejo Nacional de Investigaciones Científicas y Técnicas) and CIUNT (Consejo de Investigaciones de la Universidad Nacional de Tucumán) for financial help.

REFERENCES

[1] Tanabe Seiyaku Co. Ltd. Jpn. Kokai Tokyo Koho JP 60 51,176, *Chem. Abstr.* **1985**, *103*, 141951t.
[2] A. Salerno, I. A. Perillo, *Molecules* **2005**, *10*, 435–443.
[3] B. Szabo, *Pharmacol. Therapeut.* **2002**, *93*, 1–35.
[4] J. C. Chang, P. C. Ulrich, R. Bucala, A. Cerami, *J. Biol. Chem.* **1985**, *260*(13), 7970–7974.
[5] R. D. Enriz, E. A. Jáuregui, F. Tomas-Vert, *J. Mol. Struct. (TEOCHEM)* **1994**, *306*, 115–122.
[6] A. Salerno, V. Ceriani, I. A. Perillo, *J. Heterocycl. Chem.* **1992**, *29*, 1725–1733.
[7] R. C. F. Jones, K. J. Howard, J. S. Snaith, *Tetrahedron* **1997**, *53*, 1111–1112.
[8] P. K. Martin, H. R. Matthews, H. Rapaport, G. Thyagarajan, *J. Org. Chem.* **1968**, *33*, 3758–3761.
[9] R. E. Klem, H. F. Skinner, H. Walba, R. H. Isensee, *J. Heterocycl. Chem.* **1970**, *7*, 403–404.
[10] J. Vázquez, J. J. López González, L. Ballester, J. Boggs, *J. Mol. Struct.* **1997**, *393*, 97–110.
[11] A. E. Reed, L. A. Curtis, F. Weinhold, *Chem. Rev.* **1988**, *88*(6), 899–926.
[12] J. P. Foster, F. Weinhold, *J. Am. Chem. Soc.* **1980**, *102*, 7211–7218.
[13] A. E. Reed, F. Weinhold, *J. Chem. Phys.* **1985**, *83*, 1736–1740.
[14] R. F. W. Bader, *Atoms in Molecules, a Quantum Theory*, Oxford University Press, Oxford, **1990**. ISBN: 0198558651.
[15] F. Biegler-Köning, J. Schönbohm, D. Bayles, AIM2000; a program to analyze and visualize atoms in molecules. *J. Comput. Chem.* **2001**, *22*, 545–559.
[16] V. M. Stoyanov, M. M. El'chaninov, A. M. Simonov, A. F. Pozharski, *Khim. Geterotsikl. Soedin.* **1989**, *10*, 1396–1400.
[17] P. Pulay, G. Fogarasi, F. Pang, E. Boggs, *J. Am. Chem. Soc.* **1979**, *101*(10), 2550–2560.
[18] N. Sadlej-Sosnowska, *J. Phys. Chem. A* **2007**, *111*, 11134–11140.
[19] A. Vektariene, G. Vektaris, J. Svoboda, *11th International Electronic Conference on Synthetic Organic Chemistry (ECSOC-11), (***2007***).*
[20] CAD4. *Express Software*, Enraf-Nonius, Delft, The Netherlands, **1994**.
[21] K. Harms, S. S. Wocadlo, *XCAD4-CAD4 Data Reduction*, University of Marburg, Marburg, Germany, **1995**.
[22] G. M. Sheldrick, *SHELXS-97. Program for Crystal Structure Resolution*, University of Göttingen, Göttingen, Germany, **1997**.
[23] G. M. Sheldrick, *SHELXL-97. Program for Crystal Structures Analysis*, University of Göttingen, Göttingen, Germany, **1997**.
[24] C. K. Johnson, ORTEP-II. A Fortran Thermal-Ellipsoid Plot Program. *Report ORNL-5318, Oak Ridge National Laboratory, Tennessee, USA, (***1976***).*
[25] D. Becke, *J. Chem. Phys. Rev.* **1993**, *98*, 5648–5642.
[26] C. Lee, W. Yang, R. G. Parr, *Phys. Rev.* **1988**, *B37*, 785–789.
[27] E. D. Gledening, J. K. Badenhoop, A. D. Reed, J. E. Carpenter, F. F. Weinhold, *NBO 3.1*; Theoretical Chemistry Institute, University of Wisconsin, Madison, WI, (**1996**).
[28] B. H. Besler, K. M. Merz, Jr P. A. Kollman, *J. Comput. Chem.* **1990**, *11*(4), 431–439.
[29] 03. Gaussian, B01. Revision, M. J. Frisch, G. W. Trucks, H. B. Schlegel, G. E. Scuseria, M. A. Robb, J. R. Cheeseman, J. A. Montgomery, Jr T. Vreven, K. N. Kudin, J. C. Burant, J. M. Millam, S. S. Iyengar, J. Tomasi, V. Barone, B. Mennucci, M. Cossi, G. Scalmani, N. Rega, G. A. Petersson, H. Nakatsuji, M. Hada, M. Ehara, K. Toyota, R. Fukuda, J. Hasegawa, M. Ishida, T. Nakajima, Y. Honda, O. Kitao, H. Nakai, M. Klene, X. Li, J. E. Knox, H. P. Hratchian, J. B. Cross, C. Adamo, J. Jaramillo, R. Gomperts, R. E. Stratmann, O. Yazyev, A. J. Austin, R. Cammi, C. Pomelli, J. W. Ochterski, P. Y. Ayala, K. Morokuma, G. A. Voth, P. Salvador, J. J. Dannenberg, V. G. Zakrzewski, S. Dapprich, A. D. Daniels, M. C. Strain, O. Farkas, D. K. Malick, A. D. Rabuck, K. Raghavachari, J. B. Foresman, J. V. Ortiz, Q. Cui, A. G. Baboul, S. Clifford, J. Cioslowski, B. B. Stefanov, G. Liu, A. Liashenko, P. Piskorz, I. Komaromi, R. L. Martin, D. J. Fox, T. Keith, M. A. Al-Laham, C. Y. Peng, A. Nanayakkara, M. Challacombe, P. M. W. Gill, B. Johnson, W. Chen, M. W. Wong, C. Gonzalez, J. A. Pople, Gaussian, Inc., Pittsburgh PA, (**2003**).
[30] C. H. Surech, S. R. Gadre, *J. Org. Chem.* **1999**, *64*(7), 2505–2512.
[31] B. Ehresmann, B. Martin, A. H. C. Horn, T. Clark, *J. Mol. Model* **2003**, *9*, 342–347.
[32] T. Sundius, *J. Mol. Struct.* **1990**, *218*, 321–326.
[33] T. Sundius, *Vib. Spectrosc.* **2002**, *29*, 89–95.
[34] P. Pulay, G. Fogarasi, G. Pongor, J. E. Boggs, A. Vargha, *J. Am. Chem. Soc.* **1983**, *105*, 7037–7047.
[35] G. Rauhut, P. Pulay, *J. Phys. Chem.* **1995**, *99*, 3093–3100.
[36] G. Rauhut, P. Pulay, *J. Phys. Chem.* **1995**, *99*, 14572.
[37] F. Kalincsák, G. Pongor, *Spectrochim. Acta A* **2002**, *58*, 999–1011.
[38] A. B. Nielsen, A. J. Holder, Gauss View 3.0, User's Reference, GAUSSIAN Inc., Pittsburgh, PA, **2000–2003**.
[39] R. Ditchfield, *Mol. Phys.* **1974**, *8*, 397–409.
[40] J. Cheeseman, G. Trucks, T. Keith, M. Frisch, *J. Chem. Phys.* **1996**, *104*, 5497–5509.
[41] T. A. Keith, R. F. W. Bader, *Chem. Phys.* **1993**, *210*, 223–231.
[42] S. F. Boys, F. Bernardi, *Mol. Phys.* **1973**, *19*, 553–559.
[43] R. Fourme, *Acta Crystallogr., Sect. B. Struct. Crystallogr. Cryst. Chem.* **1972**, *28*, 2984–2991.
[44] D. Christen, S. H. Griffiths, J. Sheridan, *Z. Naturforsch.* **1982**, *37a*, 1378–1385.

[45] K. Balasubramani, P. T. Muthiah, D. E. Lynch, *J. Chem. Central* **2007**, *1*, 28.
[46] L. C. Hwang, C. H. Tu, J. H. Wang, G. H. Lee, *Molecules* **2006**, *11*, 169.–176
[47] P. T. Muthiah, S. Francis, U. Rychlewska, B. Warżajtis, *Beilstein J. Org. Chem.* **2006**, *2*, 1–8.
[48] A. Karpfen, C. H. Choi, M. Kertesz, *J. Phys. Chem. A* **1997**, *101*, 7426–7433.
[49] J. M. Granadino-Roldán, M. Fernández-Gómez, A. Navarro, L. M. Camus, U. A. Jayasoriya, *Phys. Chem. Chem. Phys.* **2002**, *4*, 4890–4901.
[50] J. R. Sambrano, A. R. de Souza, J. J. Queralt, M. Oliva, J. Andrés, *Chem. Phys.* **2001**, *264*, 333–340.
[51] S. A. Brandán, G. Benzal, J. V. García-Ramos, J. C. Otero, A. Ben Altabef, *Vib. Spectrosc.* **2008**, *46*, 89–99.
[52] I. Alabugin, M. Manoharan V. Tarek, A. Zeidan, *J. Am. Chem. Soc.* **2003**, *125*, 14014–14031.
[53] M. Montejo, A. Navarro, G. Kearley, J. Vázquez, J. J. López González, *J. Am. Chem. Soc.* **2004**, *126*, 15087–15095.
[54] F. Billes, H. Böhling, M. Ackermann, M. Kudra, *J. Mol. Struct.* **2004**, *672*(1), 1–16.
[55] S. T. King, *J. Phys. Chem.* **1970**, *74*, 2133–2138.
[56] T. D. Klots, R. D. Chirrido, W. V. Stele, *Spectrochim. Acta A* **1994**, *50*, 765–795.
[57] A. El-Azhary, R. H. Hilal, *Spectrochim. Acta A* **1997**, *53*, 1365–1373.
[58] M. E. Tuttolomondo, A. Navarro, T. Peña, A. Ben Altabef, *J. Phys. Chem. A* **2005**, *109*, 7946–7956.
[59] G. Fogarasi, X. Zhou, P. W. Taylor, P. Pulay, *J. Am. Chem. Soc.* **1992**, *105*, 7037–7047.

